Channeling of MeV Projectiles in Tungsten and Silicon

J. A. DAVIES, J. DENHARTOG, AND J. L. WHITTON
Chalk River Nuclear Laboratories, Atomic Energy of Canada Limited, Chalk River, Ontario, Canada

(Received 29 June, 1967)

Wide-angle Rutherford scattering has been used to investigate experimentally the channeling behavior of several projectiles (^{1}H, ^{4}He, ^{12}C, ^{16}O, and ^{35}Cl) in tungsten crystals in the energy region 2 to 30 MeV; the study has also been extended to silicon crystals, using a 3.0-MeV ^{1}H beam. The observed critical angles and minimum scattering yields are compared with theoretical predictions. In general, the agreement is excellent. In both W and Si, precise energy analysis of the scattered beam has also provided detailed information on the depth and temperature dependence of channeling; a marked difference is observed between the planar and axial channeling processes. Some preliminary measurements in Au and UO_2 crystals are included.

1. INTRODUCTION

MANY recent experimental and theoretical studies have established that the channeling of energetic charged particles in crystals is *not* confined only to the lower-energy region where nuclear stopping normally predominates. The proton transmission experiments of Dearnaley,[1] and the later work of Dearnaley and Sattler,[2] and of the Brookhaven–Bell Laboratory–Rutger's group,[3] show clearly that protons and alpha particles, even at MeV energies, undergo as much as a threefold reduction in their rate of energy loss, if injected along a close-packed axis or plane. Similar reductions in energy loss have also been observed by Datz *et al.*[4] for heavy ions, such as ^{79}Br and ^{127}I, at energies up to 100 MeV.

Other groups have found that those interactions requiring the projectile to pass extremely close to the nucleus—such as nuclear reaction yields,[5] Rutherford scattering,[6] x-ray production,[7] and charged particle emission from embedded radioactive nuclei[8]—exhibit even larger orientation effects and are therefore especially sensitive tools for studying channeling.

Lindhard[9] has developed an extensive theoretical framework for interpreting quantitatively this latter group of close-encounter experiments. He predicts that an energetic charged particle, moving through a crystal lattice within a certain critical angle of a close-packed axis or plane, will be steered by successive gentle collisions with the aligned rows or planes of atoms, and will not approach closer to lattice atoms than $\sim a$, the Thomas-Fermi screening distance. Hence, processes requiring smaller impact parameters than a are completely prohibited by such a steering mechanism; their yield is therefore an accurate measure of the unchanneled fraction of the beam. For this purpose, wide-angle Rutherford scattering is a particularly versatile process because it enables the energy and the atomic number of both the projectile and the target to be varied over a very wide range.

During the past few years, at the University of Aarhus, a detailed experimental investigation of channeling by means of Rutherford scattering[6] has been carried out in the energy region 50–500 keV for comparison with the theoretical predictions. An accurate comparison between experiment and theory is, of course, a necessary prerequisite for many of the applications of channeling in the solid state field.[10–12]

The present study is an extension of the Aarhus experiments to higher energies and to a wider choice of projectiles. Our main objective has been to measure accurately the critical angle for channeling along various low-index axes and planes as a function of the energy and atomic number of the projectile, and thereby to test more fully the predictions of the Lindhard theory. At the same time, since energy analysis of the back-scattered particles enables the scattering yield to be measured as a function of depth beneath the crystal surface, we have also investigated the depth dependence of the critical angle and of the number of channeled particles. In some cases, these depth studies have been extended to higher temperatures in order to investigate the influence of lattice vibrations.

Tungsten was originally chosen as the target material for the present study because our low-energy channeling work[13] had shown that it approaches most closely the ideal crystal. This can be attributed to the existence of

[1] G. Dearnaley, IEEE Trans. Nucl. Sci. **NS11**, 249 (1964).
[2] A. R. Sattler and G. Dearnaley, Phys. Rev. Letters **15**, 59 (1965).
[3] C. Erginsoy, H. E. Wegner, W. M. Gibson, Phys. Rev. Letters **13**, 530 (1964).
[4] S. Datz, T. S. Noggle, and C. D. Moak, Nucl. Instr. Methods **38**, 221 (1965).
[5] J. U. Andersen, J. A. Davies, K. O. Nielsen, and S. L. Andersen, Nucl. Instr. Methods **38**, 207 (1965).
[6] E. Bøgh and E. Uggerhøj, Nucl. Instr. Methods **38**, 216 (1965).
[7] J. M. Khan, D. L. Potter, and R. D. Worley, Phys. Rev. **148**, 413 (1966).
[8] B. Domeij and K. Bjorkqvist, Phys. Letters **14**, 127 (1965).
[9] J. Lindhard, Kgl. Danske Videnskab Selskab, Mat. Fys. Medd. **34**, 14 (1965).
[10] E. Bøgh, in *Interaction of Radiation with Solids*, edited by A. Bishay (Plenum Press, Inc., New York, 1967), p. 361.
[11] H. Matzke and J. A. Davies, J. Appl. Phys. **38**, 805 (1967).
[12] L. Eriksson, J. A. Davies, J. Denhartog, J. W. Mayer, O. J. Marsh, and R. Mankarious, Appl. Phys. Letters **10**, 323 (1967).
[13] L. Eriksson, Phys. Rev. **161**, 235 (1967); see also J. A. Davies, L. Eriksson, and P. Jespersgård [Nucl. Instr. Methods **38**, 245 (1965)].

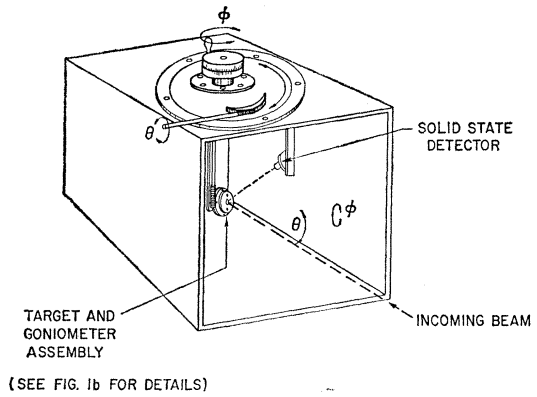

(a)

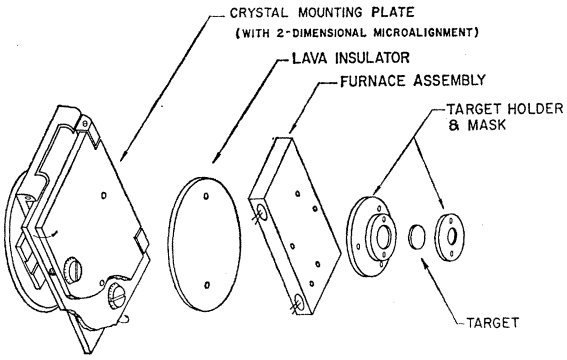

(b)

FIG. 1(a). Target chamber and rotation/tilting assembly. 1(b). Details of the goniometer assembly, including the special furnace attachment for the high-temperature runs.

a negligibly thin (<10 Å) surface oxide, and to the small value of $\bar{p}$, the rms vibrational amplitude of the lattice atoms, at room temperature.

The present study has been extended to Si in order to correlate our measurements with the extensive transmission studies of other groups.[2,3] A few exploratory measurements have also been made in Au and UO_2.

2. EXPERIMENTAL PROCEDURE

The target chamber and goniometer assembly is illustrated in Fig. 1. There are two methods for changing the target orientation with respect to the incident beam: (a) tilting the entire goniometer assembly by rotating the top flange of the target chamber, i.e., varying θ; and (b) rotating the crystal around an axis perpendicular to its mounting plate by means of the worm gear assembly, i.e., varying ϕ. θ and ϕ could be set reproducibly to 0.05 and 0.02°, respectively. The goniometer was constructed in such a way that the axes of rotation and the incident beam direction all intersect at the crystal surface.

For the high-temperature experiments, a special furnace assembly was mounted on the goniometer face [Fig. 1(b)]; even in the 500°C runs, the temperature of the main goniometer assembly did not increase significantly.

Monoenergetic beams of protons (or other low Z projectiles) were obtained from the Chalk River EN Tandem Van de Graaff. These beams were collimated to reduce the angular spread to less than 0.04° and allowed to bombard the target crystal. The backscattered yield was measured by means of a thin window (0.2 μ) solid-state detector placed just above the incident beam about 5 cm from the crystal surface. The energy resolution of the detector was 25 keV (full width at half-maximum, FWHM) for 5-MeV α particles. The mean scattering angle to the detector was 150°. The actual scattering zone "seen" by the detector consisted of a cone at least 10° wide, so as to minimize any anisotropy that might occur along the outgoing trajectory (cf. Ref. 8). This also had the advantage of providing a high counting geometry, and so enabled the beam current to be kept quite small. Typically, the beam current was $\sim 10^{-9}$ A; this produced a total counting rate of $\sim 10^4$/sec. The bombardment zone was ~ 0.1 cm^2.

To obtain information about the scattering yield as a function of depth, these backscattered particles were energy-analyzed in one of two ways: (i) the pulses were fed into a bank of six single-channel analyzers, each one being equipped with its own scaler and readout system; or (ii) the pulses were fed into a standard 100-channel analyzer. Method (i) could handle considerably higher counting rates without appreciable loss, and was used for the detailed angular scans, such

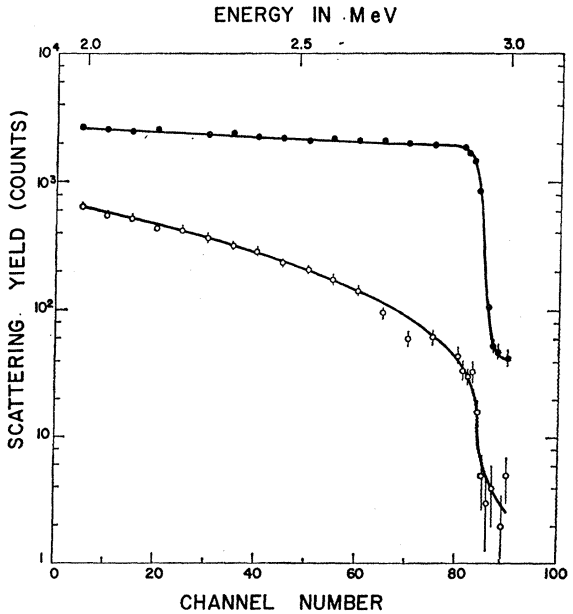

FIG. 2. Energy spectra of protons backscattered from a tungsten crystal. (●) along a random direction, and (○) along ⟨100⟩. Incident energy: 3.0 MeV.

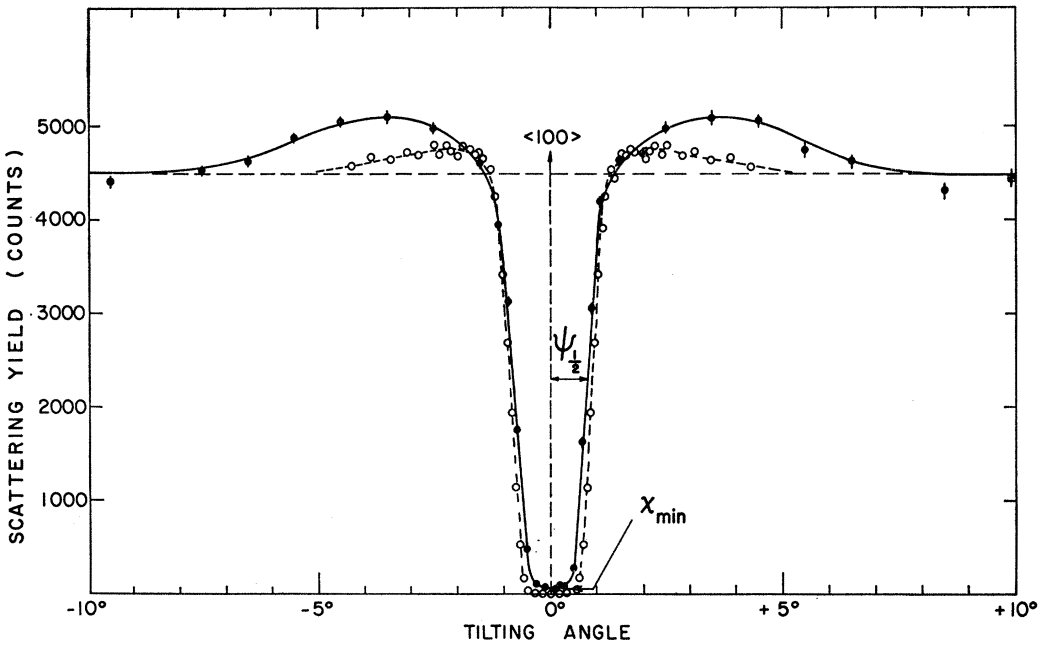

FIG. 3. Axial channeling of 3-MeV ^1H along the ⟨100⟩ in W: ● experimental data measured near the crystal surface (channels 80–85 in Fig. 2); ○ theoretical yields calculated by Andersen (Ref. 14) with the effect of lattice vibrations included. The tilting plane was carefully chosen *not* to correspond to any of the close-packed lattice planes.

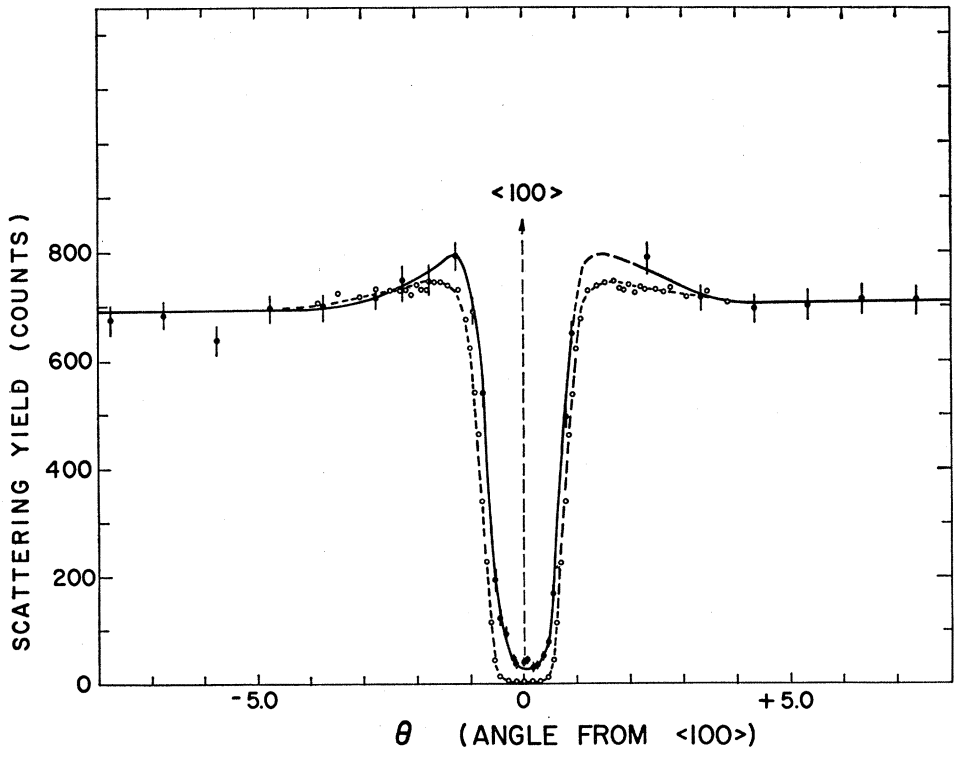

FIG. 4. Axial channeling of 30-MeV ^{16}O along the ⟨100⟩ in W: ● experimental data measured near the crystal surface (i.e., 0–8000 Å); ○ theoretical yields calculated by Andersen (Ref. 14).

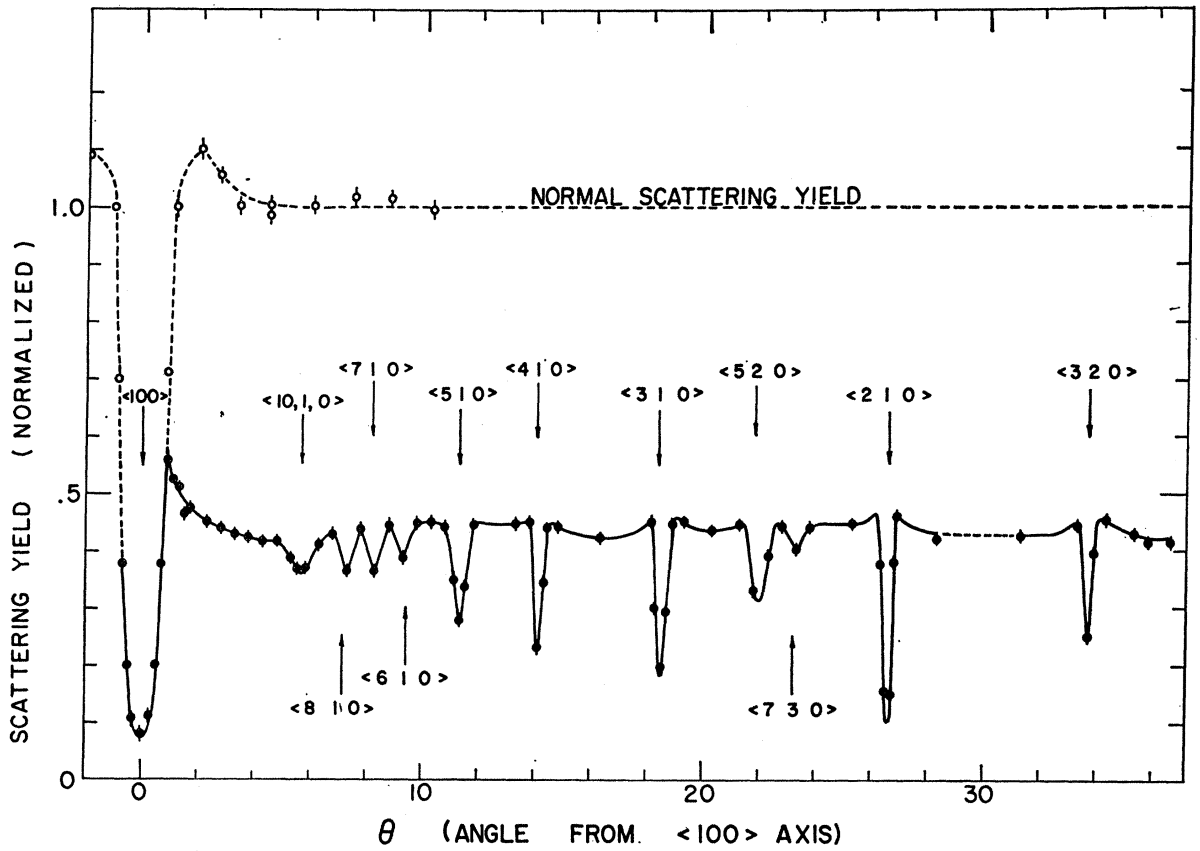

FIG. 5. Axial and planar channeling of 10-MeV ^{4}He in the {100} plane of W. ● tilting along the {100} plane; ○ tilting in a plane that does *not* correspond to any close-packed lattice plane. The measured yields are from a scattering zone about 3 μ beneath the surface.

as those in Figs. 3–8. Method (ii), on the other hand, although more time consuming, gave more detailed information on the depth dependence (Figs. 11 and 12). Typical Rutherford scattering spectra for aligned and random directions are illustrated in Fig. 2.

Each crystal had a major axis almost perpendicular to its surface. If this axis and the goniometer's axis of rotation can be made to coincide, then all subsequent orientation studies are considerably simplified. Consequently, at the start of each run, a beam of 3.0-MeV protons was used to find the exact orientation of the crystal, and a suitable correction to the crystal mounting plate was then made [(Fig. 1(b)]. Details of this pre-orientation procedure have been given previously.[5]

3. RESULTS AND DISCUSSION

3.1. Axial Effects

Figure 3 illustrates the orientation dependence of the scattering yield from just beneath the crystal surface. An extremely strong attenuation (about a factor of 80) is observed whenever the beam enters the crystal within a small angle of a close-packed row. Andersen[14] has recently developed a computer program for predicting the orientation dependence of close-encounter processes, such as backscattering. His program is based on Lindhard's theory,[9] with the effect of lattice vibrations included. As can be seen in Fig. 3, the theory predicts rather well the angular width and also the attenuation factor. A more detailed comparison with theory will be given in Sec. 4.

The shoulders occurring at larger angles confirm the existence of a significant compensation effect, but their magnitude is somewhat greater than that predicted. In fact, assuming rotational symmetry, the observed compensation in Fig. 3 is considerably greater than 100%. It should be emphasized, however, that these shoulders are sensitive to the choice of tilting plane; any slight asymmetry with respect to the various lattice planes produces an appreciable distortion in the shoulder region, although not in the dip itself. Consequently, we have not attempted to obtain quantitative information about compensation effects in the present study.

Figure 4 shows the axial effect observed with 30-MeV ^{16}O ions. Qualitatively the features are similar to those with protons (Fig. 3), and again the agreement with the theoretical yield curve is reasonable.

In Fig. 5, a different method has been used to scan through a ⟨100⟩ axis in tungsten: viz, the tilting plane

[14] J. U. Andersen, Kgl. Danske Videnskab Selskab, Mat. Fys. Medd. (to be published).

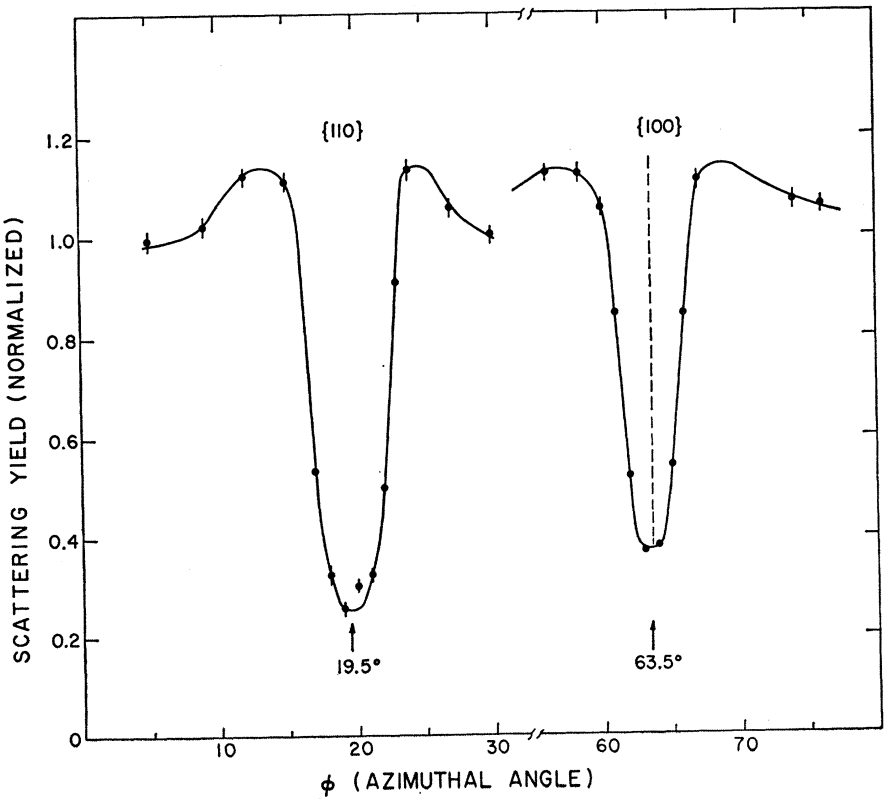

FIG. 6. Planar channeling of 3-MeV ^1H in W, measured by rotating around a ⟨100⟩ axis at a tilting angle $\theta = 5.0°$. Experimental data are the yields measured just beneath the crystal surface.

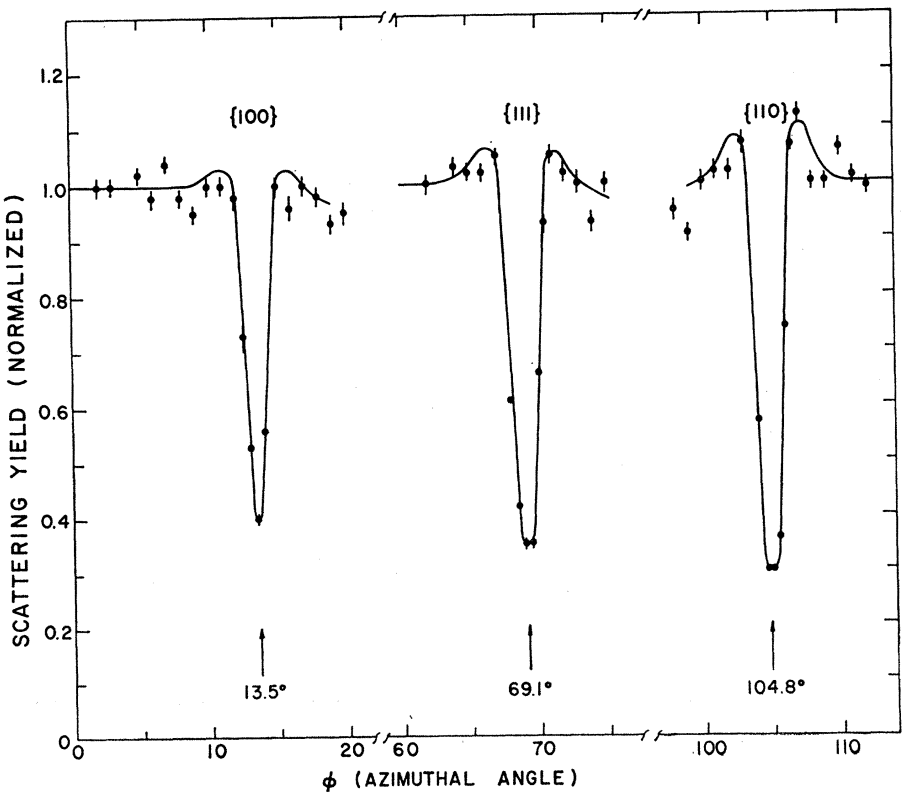

FIG. 7. Planar channeling of 3 MeV ^1H in Si, measured by rotating around a ⟨110⟩ axis at a tilting angle $\theta = 5.0°$. Experimental data are the yields measured just beneath the crystal surface.

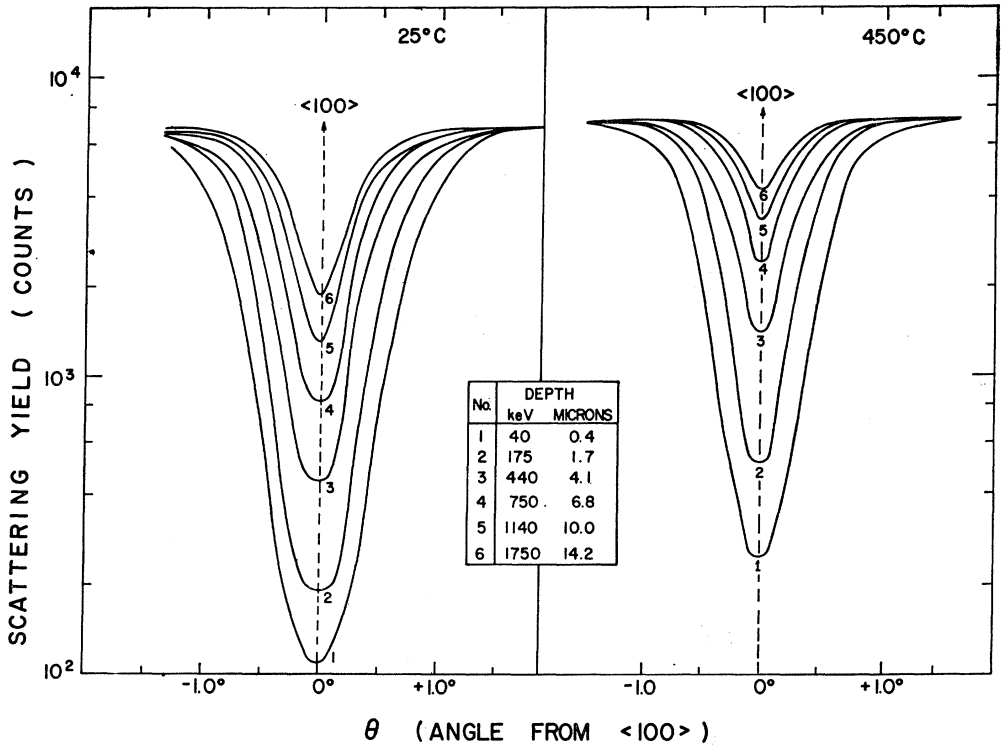

FIG. 8. Orientation scans of the scattering yield of 3-MeV protons through a ⟨100⟩ axis in tungsten at various depths beneath the surface: (a) at 25°C; (b) at 450°C. The depth in microns has been estimated from the observed ΔE values, assuming that dE/dx for the channeled beam is $\frac{1}{3}$ the "random" value.

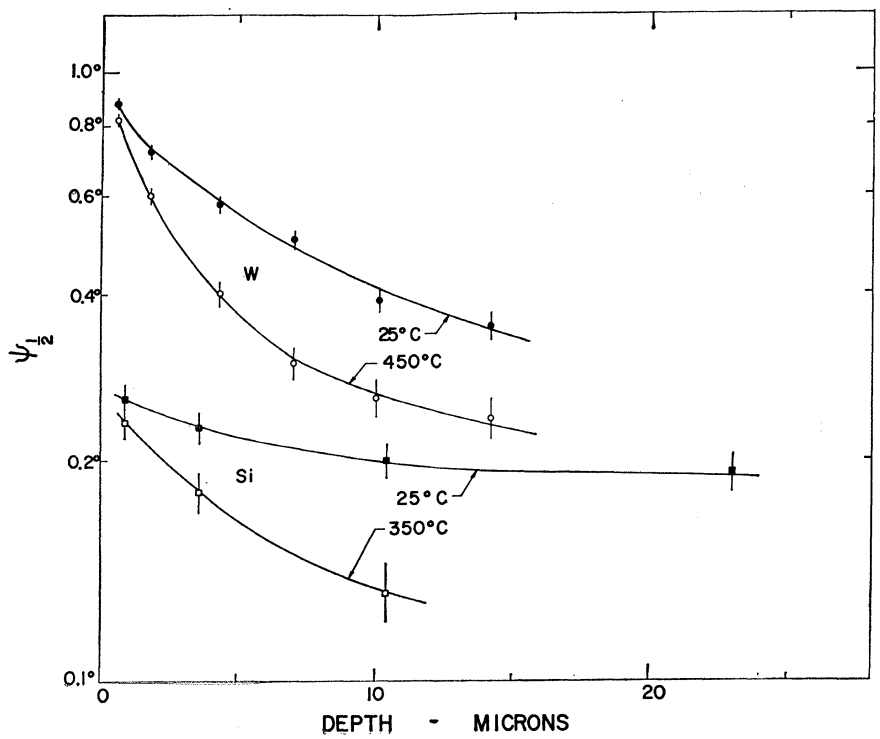

FIG. 9. Depth dependence of the critical angle $\psi_{1/2}$ for the channeling of 3-MeV protons: (a) along a ⟨100⟩ axis in W; (b) along a ⟨110⟩ axis in Si.

has been deliberately chosen to coincide with one of the close-packed lattice planes. Comparison with a similar tilt in a random plane (i.e., one that does *not* correspond to any low-index lattice plane) illustrates the relative magnitude of both axial and planar channeling. It can be seen that, within the {110} plane, the scattering yield remains constant at ~0.42 of the random value, except when the incident direction approaches one of the minor axes in the plane. It is interesting to note that even relatively high-index directions (e.g., ⟨10,1,0⟩ and ⟨7,3,0⟩) produce a measurable decrease in yield from the planar value, thereby indicating a significant increase in the channeled component. Lindhard[9] has estimated that the minimum fractional yield (χ_{min}) along an axis should be proportional to the atomic spacing d along the row, and the relative magnitude of the dips observed in Fig. 5 agrees at least qualitatively with this prediction. However, the observed values of χ_{min} for the higher-index directions (Table IV) increase somewhat more rapidly than the predicted d dependence.

It can also be seen that the angular dependence near the ⟨100⟩ is indistinguishable in the two cases until the fractional yield has risen to ~0.6 (i.e., well above the planar yield), confirming that a sharp separation exists between axial and planar channeling effects.

3.2. Planar Effects

By selecting a value of θ that does not correspond to any of the detectable minor axes, and then varying the azimuthal angle ϕ, a detailed scan through various close-packed lattice planes can be obtained (Figs. 6 and 7). Whenever the beam enters along a close-packed plane, appreciable attenuations (up to a factor of ~5) are observed; again, as in the axial case, there is evidence of compensating shoulders at somewhat larger angles. The angular widths in Figs. 6 and 7 are expressed in terms of the azimuthal angle ϕ around a 5° cone, and hence the values appear rather large. To obtain the true angular width of the planar dips, it is of course necessary to project the observed angles in Figs. 6 and 7 on to an axis perpendicular to the plane. One then obtains values of 0.1–0.3° (Table III) for the width at half minimum.

Similar rotations around each major axis have been made for θ values varying from 3 to 20°; the resulting angular widths for each plane, when projected onto an axis perpendicular to it, are independent of θ.

Andersen's computer calculations[14] are currently being extended to the planar channeling case, but are not yet available. However, a comparison with simple theoretical estimates for a nonvibrating lattice is given in the next section (Table III).

It will be seen that χ_{min} for a {100} plane in tungsten is considerably larger in Fig. 5 than in Fig. 6. The reason for this difference is that the yield in the former case is being measured at a somewhat larger depth beneath the crystal surface (cf. the depth dependence studies in Fig. 8); hence, there is no discrepancy involved.

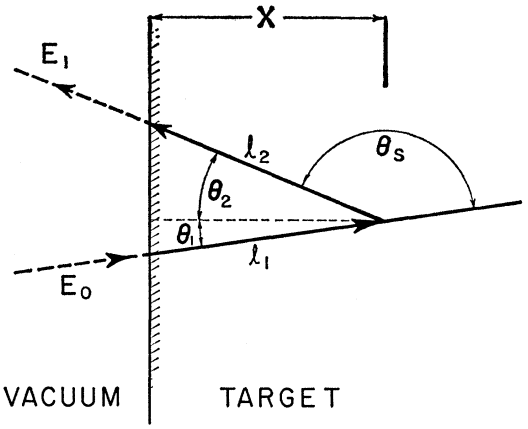

FIG. 10. Schematic diagram to illustrate the various angles involved in converting energy scales to depth scales by means of Eq. (1).

3.3. Depth and Temperature Dependence

By using the bank of single-channel analyzers described in Sec. 2, a series of orientation scans at six different depths beneath the crystal surface are obtained simultaneously. Two such scans through the ⟨100⟩ axis in tungsten at different temperatures are illustrated in Fig. 8. It is seen that the minimum scattering yield (χ_{min}) gradually increases with increasing depth, and that the angular width ($\psi_{1/2}$) at half-minimum decreases. The depth dependence of $\psi_{1/2}$ is better illustrated in Fig. 9; it is significant that, although the depth dependence is more pronounced at elevated temperatures (as one might expect), yet the extrapolated values at zero depth are almost independent of temperature.

In these experiments, the depths have been calculated by converting the energy scale of the Rutherford scattering spectrum (Fig. 2) into an equivalent depth scale (x). This is accomplished by means of the following relationship between the energy E_1 of the backscattered particle and the incident beam energy E_0:

$$E_1=\left[E_0-\int_0^{x/\cos\theta_1} S^*(E)\,dl_1\right]k_s-\int_{x/\cos\theta_2}^{0} S(E)\,dl_2 \quad (1)$$

and

$$k_s=\left[\frac{A_1\cos\theta_s+A_2}{A_1+A_2}\right]^2,$$

where k_s is the fractional energy loss on scattering, and the first and second integrals are the energy losses along the incoming and outgoing trajectories, l_1 and l_2. θ_s is the laboratory scattering angle (150° in our case), A_1 and A_2 are the masses of the projectile and target atoms, and $S^*(E)$ and $S(E)$ are the stopping powers for the aligned and random beam, respectively. The

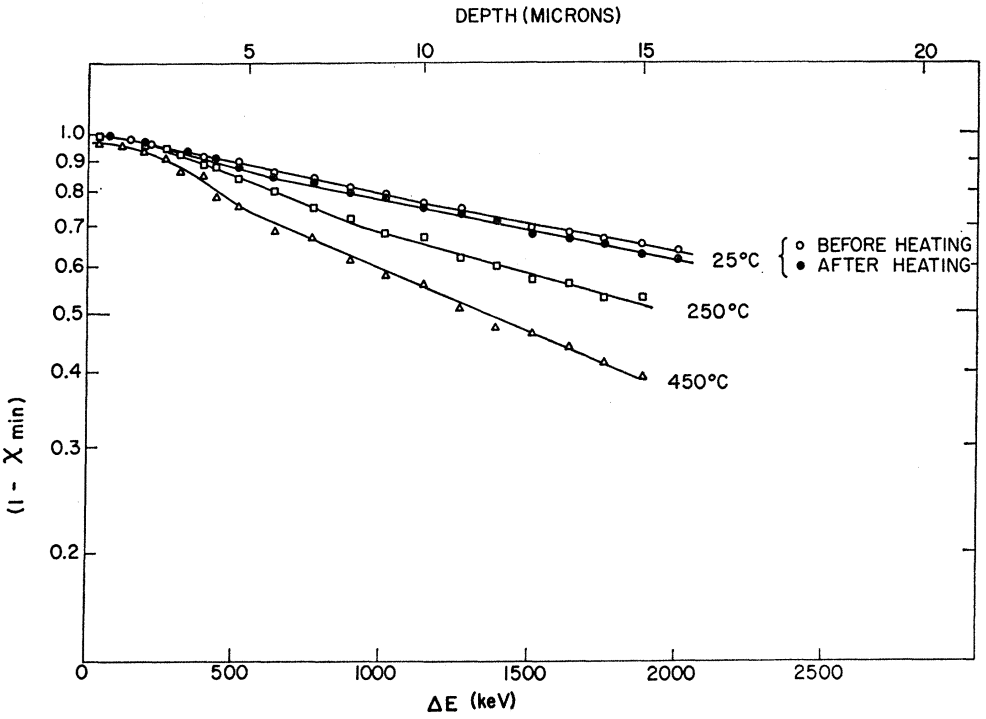

FIG. 11. Depth dependence of χ_{min} in tungsten along a ⟨100⟩ axis.

geometrical relationships between θ_1, θ_2, and θ_s are illustrated in Fig. 10.

Values of $S(E)$ for both W and Si were obtained from Whaling's compilation[15] of the available experimental data.

Values of $S^*(E)$ in the case of Si were available from the transmission experiments of Erginsoy *et al.*,[3] who reported that $S^*(E)/S(E)\sim 0.45$. In tungsten, however, the only experimental stopping power data for aligned beams are for heavier projectiles at somewhat lower velocities[16] (e.g., 1.0-MeV ^{24}Na and ^{42}K), where roughly a threefold reduction was observed. In the present W studies, we therefore assume that $S^*(E)/S(E)\sim\frac{1}{3}$. Since the major part of the energy loss occurs along the random outward trajectory, where the stopping power is accurately known, the conversion from keV to microns is not very sensitive to the above uncertainty in $S^*(E)$ for tungsten. Even if we had used a twofold or fourfold attenuation in estimating $S^*(E)$, the depth scale would only have been altered by about 12%.

In order to obtain more detailed information about the depth dependence in the perfectly aligned case, a series of spectra were obtained with a 100-channel analyzer. Figures 11 and 12 show how, at various temperatures, the channeled fraction $(1-\chi_{min})$ along an axis and along a plane decreases with increasing depth. Except for a short initial region, the observed decrease is approximately exponential. Half-thickness values ($x_{1/2}$) for this exponential region are given in Table I. It will be noted that the rate of "dechanneling" along the axes is much smaller than along the equivalent planes: e.g., in W at 25°C, ~50% of the beam remains channeled to a depth of 20 μ along the ⟨100⟩ axis, whereas at the same depth along the {100} plane the channeled component has become negligible. On

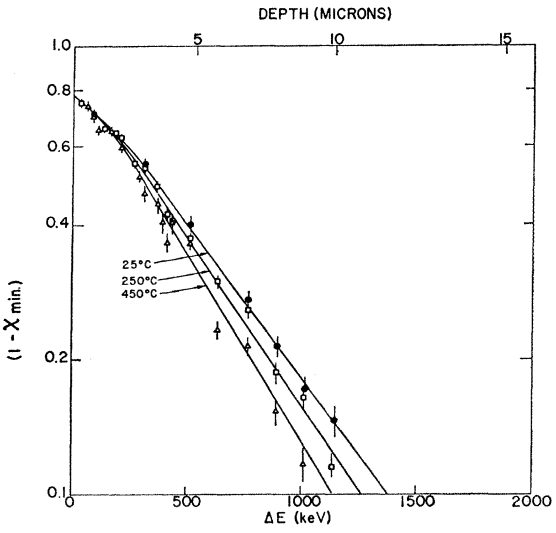

FIG. 12. Depth dependence of χ_{min} in tungsten in a {110} plane.

[15] W. Whaling, in *Handbuch der Physik*, edited by S. Flügge (Springer-Verlag, Berlin, 1957), Vol. 34, p. 193.
[16] L. Eriksson, J. A. Davies, and P. Jespersgård, Phys. Rev. 161, 219 (1967).

TABLE I. Half-thickness values $x_{1/2}$ in microns, for the exponential region of the depth dependence of χ_{min}.

Target	Projectile	Energy (MeV)	Lattice temp. (°C)	$x_{1/2}$ for axial channeling ⟨100⟩	⟨110⟩	⟨111⟩	⟨210⟩	$x_{1/2}$ for planar channeling {100}	{110}	{111}
W	^{1}H	2.0	25	20				1.3	2.7	
		3.0	25	23		44	8.0	2.8	4.1	
			250	17				2.7	3.7	
			450	12				2.3	3.5	
		6.0	25	20		40		4.0	8.8	
	^{4}He	10.0	25	14			4.0		2.5	
	^{12}C	10.0	25	>10[a]					4	
		30.0	25	16				2.4	3	
	^{16}O	10.0	25	>10[a]					4	
		30.0	25	13				1.3	3	
	^{35}Cl	30.0	25	16			3.3	1.3	1.6	
Si	^{1}H	3.0	25		11			2.3	4.5	5.0
			250		8.6			2.1	...	4.7
			350		8.0				3.7	4.0
			500		7.3				4.0	4.8
UO_2	^{4}He	5.0	25	11				4.0		
Al	^{1}H	1.4	25		~6[b]				~1.5[b]	~3[b]
Au	^{35}Cl	20.0	25	0.7						

[a] In these cases, the range of the projectile is too short to observe a measurable attenuation in χ_{min}; hence only a *lower* limit to $x_{1/2}$ can be obtained.
[b] See Ref. 5.

the other hand, the temperature dependence is much stronger in the axial case. In fact, within the estimated experimental error, our $x_{1/2}$ values for planar channeling are practically independent of temperature.

The major differences in the observed depth dependence indicate that axial channeling has a significantly different steering behavior than planar channeling, and that it cannot be represented as a simple combination of the planar effects.

The lack of any measurable temperature effect in the planar depth dependence has a fairly simple qualitative explanation. Because of the "random" distribution of lattice atoms within each aligned plane (i.e., in relation to individual particle trajectories), a channeled particle already encounters rather large force fluctuations during the steering process—even without thermal vibrations. Consequently, the extra force fluctuations introduced by lattice vibrations make a relatively smaller contribution to the rate of dechanneling than in the axial case.

Erginsoy[17,18] has recently estimated the magnitude of the temperature effect in Si by calculating the influence of lattice vibrations on the average *planar* potential, using Molière's approximation to the Thomas-Fermi potential. He predicts that, below the Debye temperature, planar channeling will be rather insensitive to temperature.

Our $x_{1/2}$ values at room temperature in tungsten and silicon are summarized in Table I, together with a few preliminary values for other crystals. In tungsten, a wide range of projectiles and energies were used; the observed values for a given axis generally agreed to within ±20%, and showed no significant dependence on either the atomic number or the energy.

[17] C. Erginsoy, Phys. Rev. Letters **15**, 360 (1965).
[18] C. Erginsoy, in *Interaction of Radiation with Solids*, edited by A. Bishay (Plenum Press, Inc., New York, 1967), p. 341.

4. COMPARISON WITH THEORY

In this section, the observed angular widths ($\psi_{1/2}$) at half minimum and the minimum yields (χ_{min}) in the perfectly aligned direction are compared with the values derived from Lindhard's theory of directional effects.[9] As the theoretical treatment does not yet permit a quantitative treatment of the depth dependence, we use only the experimental values measured just beneath the crystal surface for this comparison.

According to Lindhard, $\psi_{1/2}$ in the axial case should be proportional to a characteristic angle ψ_1 given by

$$\psi_1=(2Z_1Z_2e^2/Ed)^{1/2}, \quad \text{provided } \psi_1<a/d. \qquad (2)$$

Z_1 and Z_2 are the atomic numbers of the energetic particle and lattice atom, respectively; a is the screening distance, E the particle energy and d the lattice spacing along the chosen axis. The proportionality constant C' relating $\psi_{1/2}$ and ψ_1 (i.e., $\psi_{1/2}=C'\psi_1$) should be around 1.5–2.0 for a perfect nonvibrating crystal.

The theoretical treatment has been extended recently by Andersen[14] to include vibrational effects, as noted earlier (Figs. 3 and 4). He finds that C' for a real lattice is always significantly less than the value predicted for a perfect nonvibrating crystal, and that it decreases as the rms amplitude ($\bar{\rho}$) increases. In the case of Si, a more extensive theoretical treatment of vibrational effects has recently been given by Feldman

TABLE II. Critical angles for axial channeling at 25°C. The experimental error in $\psi_{1/2}$ is estimated to be $\pm 0.07°$.

Crystal direction	Projectile	Energy (Mev)	Predicted values ψ_1	C' [a]	$\psi_{1/2}$ [a]	Experimental values of $\psi_{1/2}$
W ⟨100⟩	^{1}H	2.0	1.05°	1.03	1.08°	1.00°
		3.0	0.86°	1.03	0.88°	0.79°
		6.0	0.61°	1.04	0.63°	0.55°
	^{4}He	2.0	1.48°	1.00	1.48°	1.39°
		10.0	0.66°	1.00	0.66°	0.67°
	^{12}C	10.0	1.15°	0.99	1.14°	1.10°
		30.0	0.66°	1.01	0.65°	0.64°
	^{16}O	10.0	1.33°	0.99	1.32°	1.23°
		30.0	0.77°	1.01	0.78°	0.70°
	^{35}Cl	10.0	1.94°	0.95	1.84°	1.82°
		30.0	1.12°	0.97	1.09°	1.00°
⟨111⟩	^{1}H	3.0	0.92°	1.03	0.95°	0.85
		6.0	0.65°	1.04	0.68°	0.52
⟨210⟩	^{1}H	3.0	0.57°	1.04	0.59°	0.51°
^{4}He		10.0	0.44°	1.04	0.46°	0.42°
^{12}C		30.0	0.44°	1.01	0.44°	0.36°
^{35}Cl		30.0	0.75°	0.96	0.72°	0.70°
Si ⟨110⟩	^{1}H	3.0	0.34°	1.11	0.38°	0.26°
					0.36° [b]	
Au ⟨110⟩	^{35}Cl	20.0	1.48°	0.72	1.07°	1.10°
UO_2 ⟨100⟩	^{4}He	5.0	0.80°	1.13	0.90°	0.55°
			0.34°	1.4[c]	0.50° [c]	

[a] Andersen's values (Ref. 14), unless indicated. [b] Reference 19. [c] Predicted values for the oxygen sublattice.

TABLE III. Critical angles for planar channeling at 25°C.

Crystal	Projectile	E (Mev)	$\psi_{1/2}$ (predicted) [a]			$\psi_{1/2}$ (experimental)		
			{100}	{110}	{111}	{100}	{110}	{111}
W	^{1}H	2.0	0.25°	0.28°		0.22°	0.26°	
		3.0	0.21°	0.23°		0.17°	0.22°	
		6.0	0.15°	0.16°		0.12°	0.18°	
	^{4}He	2.0	0.36°	0.39°		0.27°	0.38°	
		10.0	0.16°	0.175°		0.145°	0.15°	
	^{12}C	10.0	0.28°	0.31°		0.205°	0.28°	
		30.0	0.16°	0.175°		0.12°	0.16°	
	^{16}O	10.0	0.32°	0.35°		0.25°	0.33°	
		30.0	0.18°	0.20°		0.15°	0.17°	
	^{35}Cl	10.0	0.47°	0.52°		0.30°	0.42°	
		30.0	0.27°	0.30°		0.22°	0.25°	
Si	^{1}H	3.0	0.11°	0.12°	0.12°	0.070°	0.087°	0.092°
				0.15° [c]	0.13° [c]			
Au	^{35}Cl	20.0	0.36°	0.33°	0.37°	0.31°	0.24°	0.32°
UO_2	^{4}He	5.0	0.26°			0.165°	0.135°	
			0.14° [b]					

[a] Values given by $\psi_{1/2} \equiv \psi_1^*/2Z_2^{1/6}$ unless indicated. [b] Predicted value for the oxygen sublattice. [c] Reference 19.

TABLE IV. Minimum aligned yield, (χ_{min}) axial.

Crystal	Axis	Projectile	χ_{min} (predicted) Non-vibrating lattice	χ_{min} (predicted) Lattice vibrations (25°C) included	χ_{min} (observed)
W	100	^{1}H	0.0075	0.012	0.012±0.003
		^{4}He	0.007	0.011	0.025±0.005
		C, O, Cl	0.006	0.010	0.028±0.005
	111	^{1}H	0.0065	0.010	0.017±0.003
	110	^{4}He	0.011	0.018	0.025±0.005
	210	^{4}He	0.016	0.026	0.08±0.02
	310	^{4}He	0.024	0.039	0.15±0.03
Si	110	^{1}H	0.021	0.032	0.028±0.003
	111	^{1}H	0.025	0.039	0.030±0.003
UO_2	100	^{4}He	0.012[a]	0.014[a]	0.022±0.005
Au	100	^{1}H	0.006	0.026	0.07±0.02
		^{35}Cl	0.005	0.024	0.09±0.02

[a] Values for the uranium sublattice only.

and Erginsoy.[19] The two estimates of $\psi_{1/2}$ for 3.0-MeV ^{1}H in ⟨110⟩ Si (Table II) agree extremely well.

Comparison of the predicted and observed values of $\psi_{1/2}$ (Table II) shows fairly reasonable agreement in all the monatomic crystals, but not in UO_2. In the polyatomic UO_2 crystal, we have measured the scattering yield from only the *uranium* sublattice,[20] since back-scattering of ^{4}He from the *oxygen* atoms is far too weak (both in intensity and in energy) to contribute to the observed Rutherford scattering spectrum. Nevertheless, our observed $\psi_{1/2}$ value agrees with that predicted for the oxygen sublattice and not with the much larger uranium lattice value. This would suggest that multiple scattering by the oxygen is able to suppress completely the steering effect of the uranium sublattice.

TABLE V. Minimum aligned yield, (χ_{min}) planar.

Crystal	Plane	Projectile	χ_{min} (predicted)[a]	χ_{min} (observed)
W	110	^{1}H	0.10	0.18±0.02
	110	C, O, Cl	0.09	0.20±0.02
	100	^{1}H	0.14	0.30±0.03
Si	100	^{1}H	0.26	0.42±0.03
	110		0.18	0.31±0.03
	111		0.22	0.36±0.03
UO_2	100	^{4}He	0.07[b]	0.23±0.03
	110		0.10[b]	0.30±0.03
Au	100	^{1}H	0.10	0.34±0.04
		^{35}Cl	0.09	0.25±0.04
	110	^{1}H	0.14	0.43±0.04
		^{35}Cl	0.13	0.45±0.04
	111	^{35}Cl	0.08	0.27±0.04

[a] For a nonvibrating lattice.
[b] Values for the U sublattice only.

[19] L. Feldman and C. Erginsoy, Bull. Am. Phys. Soc. **12**, 391 (1967); also, L. Feldman, Ph.D. thesis, Rutgers University (unpublished).

[20] In the ⟨100⟩-directions, the UO_2 crystal consists of two different types of atomic rows — one containing only uranium atoms, the other only oxygen; hence, the lattice can be considered as two separate monatomic sub-lattices.

For planar channeling, Lindhard estimates that $(\psi_{1/2})_{planar}$ should be roughly proportional to $\psi_1^*/2Z_2^{1/6}$, where ψ_1^* is the characteristic angle of a row having the same mean lattice spacing $\bar{d}$ as the plane. Hence,

$$\bar{d}=(d_pN)^{-1/2},$$

where d_p is the spacing between the chosen lattice planes, and N is the atomic density per cm^3.

In the planar case, the influence of lattice vibrations on the proportionality constant C' has not yet been fully evaluated. However, if we assume C' to be comparable in magnitude to the mean axial value, namely $\sim$1.0, then the agreement between experiment and theory (Table III) is again fairly reasonable.

For ^{1}H in Si, a detailed theoretical treatment of planar channeling has been given by Feldman and Erginsoy.[19] Their calculated values of $\psi_{1/2}$ for the {110} and {111} planes agree quite well with those given by the $\psi_1^*/2Z_2^{1/6}$ approximation (Table III).

The other experimental parameter that can most readily be compared with theoretical predictions is the scattering yield χ_{min} of the perfectly aligned beam. At sufficiently small depths below the crystal surface, where multiple scattering effects can be disregarded, the following simple estimates have been derived:

(i) for a perfect nonvibrating lattice

$$(\chi_{min})_{axial}\simeq Nd\pi a^2, \quad (3)$$

$$(\chi_{min})_{planar}\simeq 2a/d_p, \quad (4)$$

where d is the atomic spacing *along* the axis, and d_p the spacing *between* the planes;

(ii) for a vibrating lattice, if $\langle\bar{\rho}_{xy}^2\rangle^{1/2}>a$

$$(\chi_{min})_{axial}\simeq Nd\pi\langle\bar{\rho}_{xy}^2\rangle, \quad (5)$$

where $\langle\bar{\rho}_{xy}^2\rangle$ is the mean-square amplitude of the lattice vibrations in the plane perpendicular to the aligned direction (i.e., $\langle\bar{\rho}_{xy}^2\rangle\equiv\frac{2}{3}\langle\bar{\rho}^2\rangle$). In the intermediate region, where $\langle\bar{\rho}_{xy}^2\rangle^{1/2}$ and a are comparable in magnitude, a rough estimate of χ_{min} is obtained by adding

TABLE VI. Comparison with proton scattering data from other laboratories: (i) Tulinov *et al.*[a] (ii) Feldman and Erginsoy.[b]

Direction	E (MeV)	$\psi_{1/2}$ Chalk River data	$\psi_{1/2}$ Other data	χ_{min} Chalk River data	χ_{min} Other data	$x_{1/2}$ (in microns) Chalk River data	$x_{1/2}$ (in microns) Other data
(i)							
⟨111⟩ W	3.0	0.85°	0.9°	0.017	~0.4	44	~10
	6.0	0.52°	0.6°	0.020	~0.4	40	
(ii)							
⟨110⟩ Si	3.0	0.26°	0.22° 0.25° [c]	0.028	0.073	11	11
{111} Si	3.0	0.092°	0.092° [c]	0.36		5.0	6.4
{100} Si	3.0	0.070°	0.050° [c]	0.42			
{110} Si	3.0	0.087°	0.082° 0.084° [c]	0.31	0.53		

[a] Reference 22. [b] Reference 19. [c] 11.0-MeV value multiplied by $(11/3)^{1/2}$.

the contributions from Eq. (4) and (5), namely

$$(\chi_{min})_{axial} \simeq N d\pi (a^2 + \langle \bar{\rho}_{xy}^2 \rangle). \quad (6)$$

In the planar case, the increase in χ_{min} due to lattice vibrations is much more difficult to estimate. Moreover, since Fig. 12 had indicated that temperature effects on $(\chi_{min})_{planar}$ are relatively unimportant, they have been completely omitted in the present intercomparison.

Theoretical and experimental values of χ_{min} are given in Tables IV and V for the axial and planar cases, respectively. For axial channeling, the experimental data in most cases are larger than predicted. It should be noted, however, that the discrepancy usually involves only about 0.01 of the total beam, and might therefore be caused by the imperfect nature of the crystal surface. In fact, recent experiments by Bøgh and Whitton[21] have shown that even 50 Å of oxide on a crystal surface can increase $(\chi_{min})_{axial}$ by 0.01. Furthermore, even in a perfect crystal, the scattering yield from the first (surface) plane of lattice atoms is independent of the incident beam direction, and thus contributes to the measured value of χ_{min}. With the depth resolution available in the present work, namely a few hundred atomic planes, this surface yield would add ~0.003 to χ_{min}. Hence, the agreement between experiment and theory in Table IV is quite satisfactory.

In the planar case (Table V), the experimental χ_{min} values are all significantly larger than those predicted.

In both the axial and planar cases, the energy dependence of the observed χ_{min} values was negligible.

5. COMPARISON WITH OTHER EXPERIMENTS

Tulinov *et al.*[22] also have studied the scattering behavior of MeV protons in tungsten; however, they aligned their crystal axes with the detector instead of with the incident beam, and hence have studied the so-called "blocking effect" of the scattered trajectory rather than the channeling of the incoming one. Except for the depth dependence, the "blocking" and channeling processes should be completely equivalent,[9,23] and therefore the measured $\psi_{1/2}$ and χ_{min} values should be comparable—provided they are measured close to the surface of the crystal. As can be seen from Table VI, the two sets of $\psi_{1/2}$ values do in fact agree quite well, but Tulinov *et al.*'s χ_{min} data are at least a factor of 10 larger than ours; this may be attributed to the much poorer depth resolution in their work. They also observe a much more pronounced depth dependence.

Recently, the Bell Laboratories–Brookhaven–Rutger's group[19] have extended their ^1H transmission experiments in Si to include Rutherford-scattering measurements. Their values of $\psi_{1/2}$ and $x_{1/2}$ agree extremely well with our 3-MeV data (Table VI). The small discrepancy in the χ_{min} values is probably due to a small difference in the depth resolution between the two sets of measurements.

ACKNOWLEDGMENTS

We are most grateful to our colleagues at Chalk River and at the University of Aarhus, particularly J. Lindhard and J. U. Andersen, for their stimulating discussions and encouragement. A special thanks is extended to J. U. Andersen and to C. Erginsoy and L. Feldman for having given us the results of their computer studies prior to publication. The technical assistance of G. Sims and D. A. S. Walker and of the Chalk River National Laboratory Tandem accelerator group has been most valuable throughout this experimental program.

[21] E. Bøgh, in Proceedings of the Solid State Physics Research with Accelerators Conference (Brookhaven, N.Y.) (to be published).

[22] A. F. Tulinov, V. S. Kulikauskas, and M. M. Malov, Phys. Letters **18**, 304 (1965).

[23] E. Bøgh and J. L. Whitton, Phys. Rev. Letters **19**, 553 (1967).